PROCEEDINGS REPRINT

SPIE—The International Society for Optical Engineering

Reprinted from

Infrared Technology and Applications XXII

8–12 April 1996
Orlando, Florida

Volume 2744

SHIPIR/NTCS: a naval ship infrared signature countermeasure and threat engagement simulator

D.A. Vaitekunas, K. Alexan, O.E. Lawrence

W.R. Davis Engineering Limited, 1260 Old Innes Road,
Ottawa, Ontario, Canada, K1B 3V3
e-mail: ntcs@davis-eng.on.ca

F. Reid

Defence Research Establishment Valcartier, Electro-Optics Division,
P.O. Box 8800, Courcelette, Québec, Canada, G0A 1R0

ABSTRACT

An integrated naval infrared target, countermeasure and threat model is presented. The target modelling capabilities include complex 3-D surface geometries, a thermal system model with auto-generated solar heating, sea/air convection, sea/sky radiation and inter-surface radiation, a surface radiance model which accounts for multiple diffuse reflections, observer-to-target atmospheric absorption and path radiance, and an exhaust gas dispersion and IR emission model. The IR images of any number of targets can be rendered simultaneously within a full-hemispherical sea/sky/sun background relative to an observer at a specified altitude, based on the atmospheric radiance, solar irradiance, path radiance and time-average solar sea-glint. Flare countermeasures are added to the scenario through definition of canisters, submunitions, burn characteristics and deployment tactics. The IR missile model has been constructed from a minimum number of parameters to keep the model generic and provide a reasonable estimate of IR susceptibility. The purpose of the model is to provide the tools necessary to develop and assess the effectiveness of infrared signature suppression and infrared countermeasures. A number of analysis methods are provided, including on-screen image analysis, polar signature plots, polar lock-on range and engagement simulation.

Keywords: infrared, target, threat, countermeasure, signature, detection, engagement, tactics.

1. INTRODUCTION

Infrared-guided (IR) missiles represent a major threat to military platforms, whether on land, at sea or in the air. With the development of more sophisticated IR detection and tracking systems, this threat will only increase. All platforms are potential IR targets due to the inherent IR signatures associated with internal heat transmission, external surface heating or visible hot metal and exhaust gas plume emission from power plants. Various methods of infrared signature suppression (IRSS) are available, including thermal insulation, low-emissivity paints, optical blockage, surface film-cooling and exhaust-gas cooling. Although IRSS can significantly reduce and, in some cases, eliminate IR signature, they can not always provide adequate protection under all operating conditions. Hence, infrared countermeasures (IRCM) such as flare decoys have become essential in deterring the IR threat.

The challenge facing the designers of both IRSS and IRCM systems is to determine what levels of IRSS and IRCM are adequate, taking into account costs and benefits. The large variation in area and IR intensity of an extended target such as a naval ship makes it more difficult to assess the critical components of IR signature. Developing IR flares with the proper burn characteristics, launch pattern and submunitions is also more difficult in the case of ships. The ultimate goal is to minimize ship signature and match an IR flare countermeasure with an effective deployment strategy to the resultant signature. To achieve this, a comprehensive signature and countermeasure analysis tool is required.

0-8194-2125-1/96/$6.00

SHIPIR/NTCS[1,2,3,4,5] offers an integrated simulation and modelling environment for IRSS/IRCM development and assessment. The target modelling features of SHIPIR provide analytical prediction of target surface temperature, target radiance, exhaust gas plume dispersion and plume IR emission. NTCS integrates the results of SHIPIR into a multi-target, multi-flare, naval IR background simulation environment. On-screen analysis features, such as polar signature and polar lock-on range, form a basis on which to assess IRSS effectiveness. The ability of NTCS to configure a multi-target and multi-flare scenario and simulate their engagement with various types of IR threats provides an effective means to assess IR flare designs and deployment tactics.

2. OVERVIEW

2.1 IR scene components

The NTCS scene, as illustrated in the wireframe of Figure 1, consists of various sea, sky, sun, target and plume surfaces. Although not displayed, the IR scene can also contain IR flares. The sea, sky and sun are auto-generated based on computations from either LOWTRAN7[6] or MODTRAN3[7]. For the sea surface, a solar sea-glint model by Cox and Munk[8] is used.

Considerable effort is required to define a target surface geometry, but the exhaust gas plume geometry is auto-generated from a basic set of inputs. The plume surfaces are treated differently from all other surfaces as they must volumetrically absorb and emit IR radiation. To account for this phenomena, a series of isothermal plume *shells* are generated which are raytraced and rendered through pixel image processing.

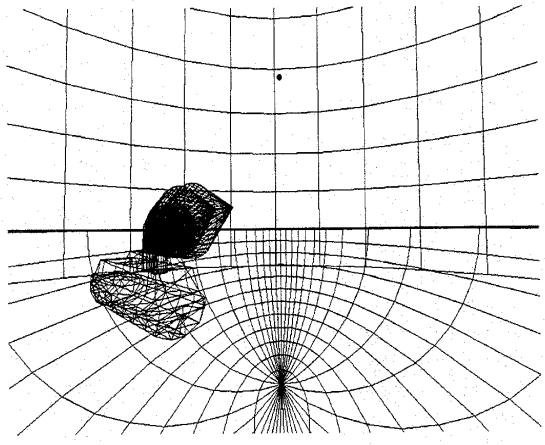

Figure 1: NTCS IR-wireframe scene.

The IR-rendered scene corresponding to the previous wireframe is shown in Figure 2. The image serves to illustrate the solar reflection off the sea and the exhaust gas plume emission. The side of the ship in view is shaded from the sun so that a view from the other side of the ship would show a significant rise in target signature due to solar heating.

2.2 IR component models

The various SHIPIR/NTCS model components and their functional relationship are shown in Figure 3. The background, target, missile and flare are characterized through their model input parameters. Various components of the background and target model which make use of other programs or require a significant amount of computation are pre-processed outside of NTCS.

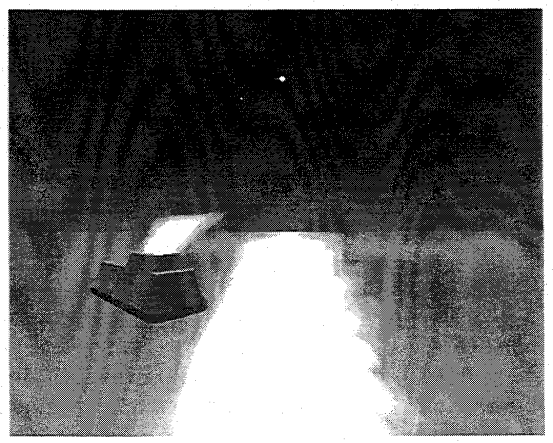

Figure 2: NTCS IR-rendered scene.

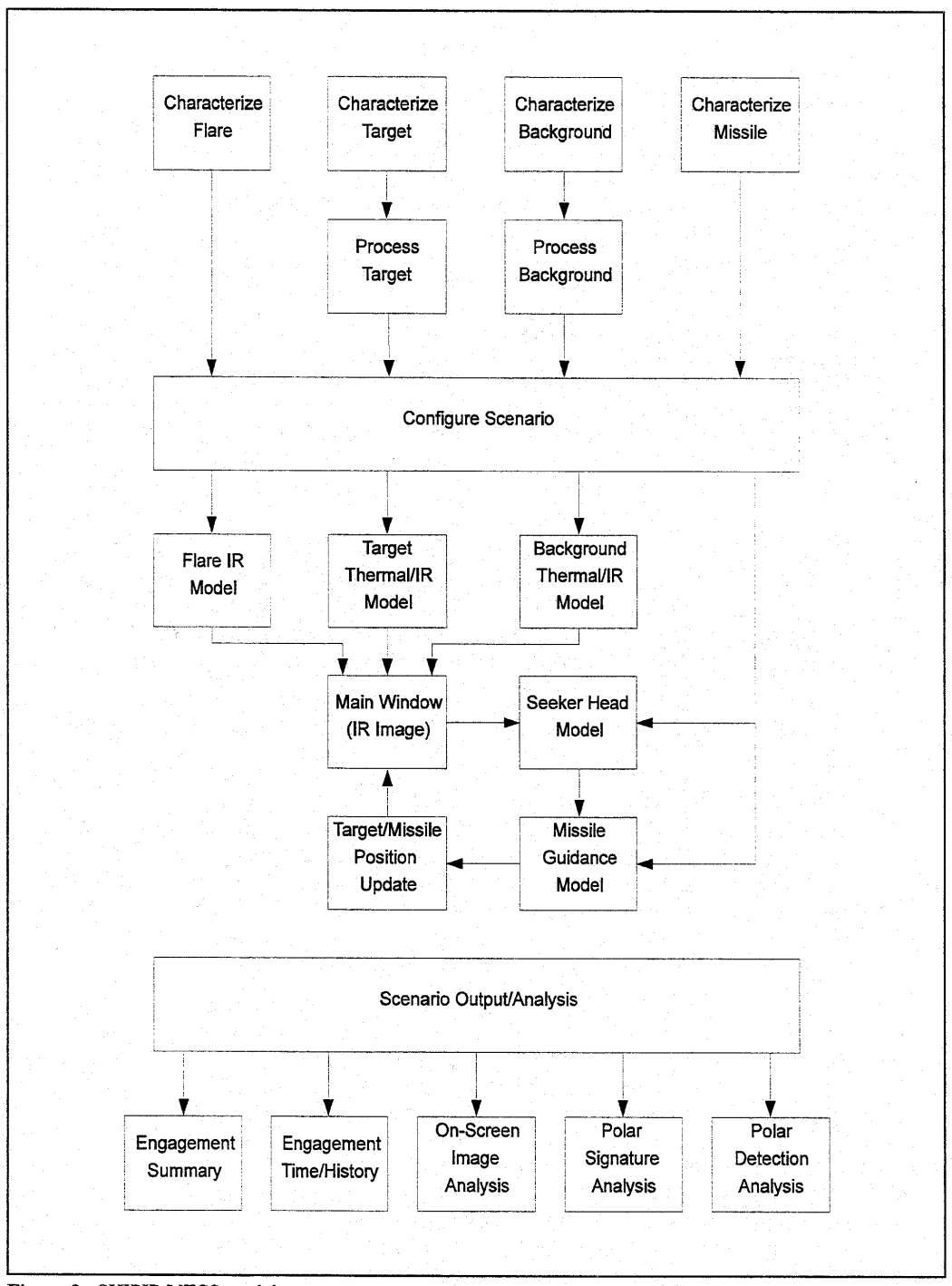

Figure 3: SHIPIR/NTCS model components.

The target(s), their flare inventories, the background and missile are then loaded into an NTCS *scenario*. Based on the relative position of these scenario components and the observer, the display routines render an IR image in the main window, as shown in Figure 2. The main IR image is passed into the seeker head model for signal processing, where various detection, tracking and aim-point algorithms are implemented. The resultant aim-point is used by the missile guidance algorithm to steer the missile along a correctional heading. Finally, the relative positions of all scene objects, including the missile, are updated based on their current heading and speed. The integrity of the background, as viewed from the missile, is maintained by moving it with the missile through each positional update. The full-hemispherical nature of the background makes it applicable to any view angle. A number of analysis and reporting features are available.

3. BACKGROUND MODEL

The background is defined by its geography, atmospheric profile and cloud data, ambient sea/air conditions and various observer-related parameters such as altitude and IR waveband. This section describes the methods used to evaluate the thermal and radiative components of the background. Each model component is calculated in-band to render the IR image for the specified observer waveband (i.e., 3-5μm, 8-12μm). The same calculations are extended to the entire IR spectrum (0.2-14μm) for use in calculating the thermal radiative exchange between target and background.

3.1 Sky

The sky consists of spectral radiances (L_{sky}) obtained using either LOWTRAN or MODTRAN. The radiance is a function of observer altitude, zenith angle (θ) measured from the vertical and, in the case of solar scattering, azimuth angle (α). The results are integrated spectrally to obtain the in-band and total sky radiances. The in-band sky radiances are mapped to a hemispherical dome with a radius of 50 km to be used in the IR image. The sky irradiance of both target and sea are determined by integrating the sky radiances over the hemisphere:

$$E_{sky} = \int_{\alpha=0}^{2\pi} \int_{\theta=0}^{\frac{\pi}{2}} L_{sky} \cos\theta \sin\theta \, d\theta \, d\alpha$$

3.2 Sun

The sun consists of a spectral irradiance (E_{sun}) obtained from either LOWTRAN or MODTRAN and integrated spectrally to obtain the in-band and total solar irradiance. The key parameters affecting solar irradiance are date, time, geographic location, atmospheric profile and observer altitude. The solar radiance (L_{sun}) is computed for an equivalent sphere located at the 50 km sky radius using the following solid angle relation:

$$L_{sun} = \frac{E_{sun}}{\omega_s} = \frac{E_{sun}}{\left(\frac{A_n}{R^2}\right)} = \frac{E_{sun}}{\pi} \frac{R_s^2}{r_s^2} = 5{,}683\, E_{sun}$$

3.3 Sea

The IR emissions of the sea consist of direct thermal emission, diffuse sky reflections, specular solar reflections, all of which are spectrally transmitted through the sea-to-observer path along with the atmospheric path radiance. The sea geometry is discretized using the Cox and Munk sea-azimuth angle (α^*) and the sea-tilt angle (β^*). These angles define a wind-referenced coordinate system located at the point of specular sea reflection ($\beta^*=0$) and

covering the sea surface up to the maximum tilt angles at the horizon. Once the sea geometry has been determined, the sea radiances are computed using the following relation:

$$L_{sea}(\alpha^*,\beta^*) = \tau(R)\left[\left(1-f(\beta^*,W)\right)L_b(T_{sea}) + f(\beta^*,W)\frac{E_{sky}}{\pi} + \rho(\omega)g(\beta^*)S(\beta^*,W)P(\alpha^*,\beta^*)L_{sun}\right] + L_{atm}(R)$$

where τ is the atmospheric path transmittance and L_{atm} the atmospheric path radiance. The diffuse hemispherical sea reflectance (f), the Lambertian surface radiance (L_b), the specular sea reflectance (ρ), the geometric scattering factor (g) and the sea-slope shadowing factor (S) are all taken from Cox and Munk, and Saunders[9]. The probability of a specular reflection (P) at a sea vertex is determined from the Gram-Charlier probability density distribution derived by Cox and Munk:

$$p(Z_u,Z_v,W) = \frac{1}{2\pi\sigma_u\sigma_v}\exp\left[\frac{-(\zeta^2+\eta^2)}{2}\right](1-C(W)); \qquad \zeta = \frac{Z_v}{\sigma_v}; \qquad \eta = \frac{Z_u}{\sigma_u}$$

where Z_u, Z_v, W are the component sea slopes and wind speed, respectively. Numerically integrating the probability density in the vicinity of a sea vertex results in:

$$P(\alpha^*,\beta^*) = \int_{\Delta A}\int p(Z_u,Z_v,W)\,dZ_u\,dZ_v$$

Similar to the sky, the sea radiances are integrated over the observer-to-sea azimuth (α) and elevation (β) angles up to the horizon ($\beta=\beta_T$) to compute the hemispherical average sea irradiance:

$$E_{sea} = \int_{\alpha=0}^{2\pi}\int_{\beta=0}^{\beta_T} L_{sea}\cos\beta\sin\beta\,d\beta\,d\alpha$$

Currently, only the diffuse components of the sea irradiance are considered.

3.4 Atmosphere

As noted in the sea model, the spectral atmospheric path radiance (L_{atm}) and spectral transmittance (τ) from the observer to the sea are required. These are obtained using either LOWTRAN or MODTRAN along a series of slant paths. The resultant look-up table as a function of range and wavelength is interpolated and used to calculate both the sea and target radiances. The resultant path geometry is also used to correct the sea surface curvature for atmospheric refraction.

4. TARGET MODEL

This section describes the target modelling features of SHIPIR with an emphasis on the key theory and procedures involved. The targets are defined from their 3-D surface geometry. These surfaces are grouped into isothermal zones, each zone sharing the same temperature. The isothermal zones form the basis of an auto-generated thermal system model (TSM) which accounts for the solar heating, sea/air convection, sea/sky radiation and inter-surface radiation. A utility exists to add the internal (user-defined) thermal boundary conditions (TBC) which include ventilated enclosures, thermal insulation, convection, specified temperature and heat flux. Each target surface forms the basis of a radiative model which is resolved both thermally and in-band to compute the target radiance. A plume model, which includes various gas-temperature and gas-constituent dispersion correlations, is used to calculate the spectral radiative gas emission and absorption along various lines-of-sight from the observer to the target. These results are rendered into the IR image using specialized image processing techniques.

4.1 Thermal model

The target thermal model is derived from the following generalized heat conduction equation:

$$C\frac{\partial T}{\partial t} = K\frac{\partial^2 T}{\partial x^2} + S$$

where C is the thermal capacitance, K the thermal conductivity and S the heat-source term. The above equation can be formulated as a finite difference (FD) equation centered about each isothermal zone:

$$D_i\frac{dT_i}{dt} + \sum_j^{N_j^i} C_{ij}(T_i - T_j) + \sum_l^{N_k^i} Q_{ik} = 0$$

$D_i=(mC_p)_i$ is the mass-capacitance of the zone, C_{ij} the inter-zonal conductances and Q_{ik} the inter-nodal heat flux. The conductances are due to either conduction or convection and the heat flux due to either heat-sources or radiation:

$$C_{ij} = \begin{cases} (KA/t)_{ij} \\ (hA)_{ij} \end{cases} \qquad Q_{ik} = \begin{cases} (qA)_{ik} \\ \sum_l^{N_l^i} \left[\sum_m^{N_n^l} A_l F_{lm}(J_l - J_m) \right] \end{cases}$$

A is the area for conductance or heat-flux and h the convective heat transfer coefficient. The terms F and J are defined in the radiative model. For the steady-state thermal solution the above FD equation is simplified to:

$$\sum_j^{N_j^i} C_{ij}(T_i - T_j) + \sum_l^{N_k^i} Q_{ik} = 0 \quad \Rightarrow \quad T_i = \frac{\sum_j^{N_j^i} C_{ij} - \sum_l^{N_k^i} Q_{ik}}{\sum_j^{N_j^i} C_{ij}}$$

4.2 Radiative model

By applying radiative materials and their associated emissive/reflective characteristics to each surface element of the target, a radiative model has been formulated which considers multiple diffuse reflections, radiative exchange with the background and incident solar radiation. The model uses the concept of *radiosity* which is defined as the net (emitted and reflected) radiation leaving a surface:

$$J_i = \epsilon_i M_{b,i} + \rho_{D,i}\left(F_{i,sky}E_{sky} + F_{i,sea}E_{sea} + F_{i,sun}E_{sun} + \sum_j^{N_j} F_{ij}J_j\right)$$

where M_b is the blackbody exitance and ρ_D the diffuse reflectance. F_{ij} are the radiative view factors or shape factors, denoting the portion of diffuse radiation leaving one surface and reaching another. Their formulations are well described elsewhere[1,5,10]. By expressing the net radiative loss from the surface in terms of a net exchange in radiosity:

$$q_{i,rad} = F_{i,sky}(J_i - E_{sky}) + F_{i,sea}(J_i - E_{sea}) - F_{i,sun}E_{sun} + \sum_j^{N_j^i} F_{ij}(J_i - J_j) = \frac{Q_{i,k}}{A_i}$$

a direct coupling is made between the thermal and radiative model which must be resolved simultaneously. Once the radiosity has been solved, the target radiances are simply defined as:

$$L_i = \tau_{atm} \frac{J_i}{\pi} + L_{atm}$$

The path radiance and transmittance are incorporated into the patch radiance since they will also determine its colour in the IR image.

4.3 Plume model

Exhaust gas plumes are normally characterized by the ejection of an axisymmetric flow of hot gas into a cool ambient air-stream. A combination of momentum and buoyancy forces act on the hot gases to disperse their concentrated thermal energy and combustion by-products which produce IR emissions. As such, plume signatures are largest at the exhaust stack exit. Various empirical correlations by Blevins[11] and Baham and McCallum[12] are used to model three different types of plume dispersions. An axisymmetric jet plume is formed when the plume flow-field is dominated by free-stream velocity, usually that of the target itself. A vertical 2-D plume results when a plume exits into an almost stagnant air-stream and the initial stack momentum is lost to buoyancy, producing a vertical plume rise. A horizontal 3-D plume is the most typical for ships, where the exhaust gas exits into a cross-wind and both momentum and buoyancy dominate the flow field. These correlations define the centreline path trajectory as well as the centreline and radial temperature and species concentration:

$$\phi_c = \frac{\psi_c - \psi_\infty}{\psi_g - \psi_\infty} = f(S) \qquad \phi_r = \frac{\psi_r - \psi_\infty}{\psi_c - \psi_\infty} = f(r/R)$$

where Ψ denotes either temperature or composition and the subscripts c, r ∞, g refer to the centreline, radial, ambient and exit conditions. The centreline distribution is mainly a function of trajectory path length while the radial distribution is Gaussian. Exhaust gas IR emission and transmission are calculated using the previous work of Romaniuk and Birk[13]. Spectral radiance and transmittance of a combustion gas are calculated through a finite number of isothermal, iso-concentration layers using the following difference equation:

$$L_g(\lambda) = \int_{z_1}^{z_2} L_g(\lambda, z)\, dz = L_{g,n}(\lambda) = \Delta L_{g,n}(\lambda) + \Delta\tau_{g,n}(\lambda) L_{g,n-1}(\lambda)$$

$$\tau_g(\lambda) = \int_{z_1}^{z_2} \tau_g(\lambda, z)\, dz = \Delta\tau_{g,n}(\lambda) \times \tau_{g,n-1}(\lambda) \qquad , \quad n = 1, N_z$$

The emission and transmittance of each layer are defined as:

$$\Delta L_{g,i}(\lambda) = f\,(T_i\,,\, p_{CO_2,i}\,,\, p_{H_2O,i}\,,\, p_{CO,i}\,,\, p_{O_2,i}\,,\, p_{N_2,i})$$
$$\Delta\tau_{g,i}(\lambda) = f\,(T_i\,,\, p_{CO_2,i}\,,\, p_{H_2O,i}\,,\, p_{CO,i}\,,\, p_{O_2,i}\,,\, p_{N_2,i})$$

which are functions of both the temperature and constituent partial-pressures. Like the target, the plume radiances are adjusted spectrally for atmospheric attenuation and path radiance. Although the model uses a simple band-model, when MODTRAN is used for the atmosphere, it has been shown to re-produce the measured trends[5].

A unique method has been developed to render the plume within the IR image. First, the plume isotherm shells are raytraced and the resultant multi-layer paths used to compute the in-band gas radiance and transmittance at each vertex on the outer surface of the plume. The plume surface is rendered as a solid, once using the coloured radiances and once using the coloured transmittances. The original image, without the plume, and the two plume images are combined pixel-by-pixel using:

$$L_p'[i] = L_g[i] + \tau_g[i] \times L_p[i] + (1 - \tau_g[i]) L_{atm}$$

The L_{atm} term is a compensation for the path radiance already in the image being attenuated by the plume.

5. FLARE MODEL

The flare model in NTCS uses an equivalent blackbody in-band emission with an exponential rise and decay to calculate intensity over time:

$$L_{Flare}(t) = L_b(T_{Flare}) \times f(t) \qquad f(t) = \begin{cases} 1 - e^{-t/\tau_r}, & 0 \le t \le t_r \\ e^{-(t-t_r)/\tau_b}, & t_r < t \le t_b \end{cases}$$

where t_r, t_b, τ_r and τ_b are the rise-time, burn-time, rise time constant and burn time constant, respectively. The flares are represented geometrically by a 2-D circular disc kept normal to the observer. The spatial variation in flare intensity is handled by randomly generating the pixel location uniformly over the flare circle until the desired coverage area is obtained:

$$F_n = F_{n-1} + k(1 - F_{n-1})$$

where n is the n-th pixel being rendered, F_n is the accumulative coverage (%) and k is the ratio of pixel area to total flare area. Like the target, the intensity of the flare is adjusted for atmospheric attenuation and path radiance.

The effects of gravity and wind on the flare are modelled by a constant sink rate and the following drag force:

$$F_D = (\tfrac{1}{2} \rho V_\infty^2 S)\ C_D$$

where ρ, V_∞, S and C_D are the air density, wind velocity, frontal particle area and drag coefficient, respectively. The flare is deployed using a canister and submunition structure. Like the real flare, a canister is launched with each submunition igniting within consecutive time delays. Each submunition is rendered separately using the above intensity, coverage and drift relations. Pre-ignition flight is not modelled; instead, a launch azimuth, distance from the target and altitude is used to locate each submunition at ignition. By selecting the proper time delays and launch range, the submunitions can appear in a stationary pattern or moving pattern, independent of the target motion.

6. MISSILE MODEL

The methods used to model the seeker head and missile guidance in the NTCS missile engagement have been previously described by Vaitekunas et al.[4]. The key relations and any modifications made to the model are discussed below.

6.1 Seeker head parameters

The seeker head parameters consist of a minimum set of design parameters necessary to describe the optical and detector design of the missile. A sampling frame rate (f_T) for the seeker simulation is governed by the maximum miss distance (y_{max}) at the minimum range of manoeuvrability (R_i) with maximum acceleration ($a_{m,max}$):

$$\frac{1}{f_T} = T_f \approx \frac{\tau_i}{5} = \frac{1}{5}\left(\frac{R_i}{2V_c}\right) = \frac{1}{10}\sqrt{\frac{2y_{\max}}{a_{m,\max}}}$$

Typically, a frame rate of 16 Hz is sufficient for naval ship engagements. The overall seeker field of view (FOV) and instantaneous FOV requirements are based on the maximum horizontal and vertical miss-distances at the minimum range of manoeuvrability and the anticipated "hot spot" size at the maximum detection range:

$$FOV_x = \sin^{-1}\left(\frac{X_{\max}}{R_i}\right) \qquad FOV_y = \sin^{-1}\left(\frac{Y_{\max}}{R_i}\right)$$

$$IFOV_x = \sin^{-1}\left(\frac{X_{hot\ spot}}{R_{\max}}\right) \qquad IFOV_y = \sin^{-1}\left(\frac{Y_{hot\ sport}}{R_{\max}}\right)$$

From the FOV and IFOV specifications, the detector array resolution is calculated as $NP_x=FOV_x/IFOV$ and $NP_Y=FOV_Y/IFOV$, where a square IFOV is typically chosen for the seeker. A noise-equivalent-radiance (NER) is calculated for the seeker using the relation:

$$NER = \frac{NEP}{A_{eff,\ ap}\ IFOV} \approx \left(\frac{2.8}{\pi}\right) \frac{\sqrt{IFOV\ \Delta f}}{D_o\ \tau_{opt}\ D^*_{hemi}\ IFOV}$$

based on the noise-equivalent-power (NEP), the effective aperture area ($A_{eff,\ ap}$), the aperture diameter (D_o), an optical transmission factor (τ_{opt}), a noise-equivalent bandwidth (Δf) and an average hemispherical detectivity (D^*_{hemi}). If n detectors are used to scan the seeker's field of view, then:

$$\Delta f \approx \frac{FOV}{T_f\ IFOV\ n\ K_s}$$

where K_s is the scanning efficiency.

6.2 Signal processing

The seeker head signal processing operates off the main window IR image which has a built-in image intensity algorithm to ensure the most intense pixel (L_{max}) remains within the top 10% of the 4096 colour map entries used to render the IR image. In the first stage of the seeker, the main image ranging in radiance form (0-L_{max}) is converted to an equivalent seeker raw image (0-L_{agc}), taking into account the detector resolution. An automatic gain control algorithm based on the work of Morin et al.[14] is used to adjust the L_{agc} of the seeker window. A second stage generates a line-by-line contrast radiance image upon which detection and tracking are performed.

Using a signal-to-noise ratio (SNR) and the NER specified in the missile input, the contrasted image is scanned for detection using the following criteria: (1) a minimum number of pixels must satisfy the condition that pixel contrast radiance exceed SNRxNER; (2) a minimum number of detected pixels must remain in that state for a minimum number of consecutive frames. If at any time, the seeker loses detection, the criteria are reset and the process begins again. The three most basic tracking algorithms[15] have been implemented: binary centroid, intensity centroid and threshold intensity centroid. Once detected, a 2-D seeker aim-point is calculated and passed onto the missile guidance algorithm.

6.3 Missile guidance

The 2-D aim-point (X_A, Y_A) and image centre (X_C, Y_C) are used to calculate an aim-point vector:

$$n_{Ax} = \frac{C_{Ax}}{\sqrt{1 + C_{Ax}^2 + C_{Ay}^2}} \qquad n_{Ay} = \frac{C_{Ay}}{\sqrt{1 + C_{Ax}^2 + C_{Ay}^2}} \qquad n_{Az} = \frac{1}{\sqrt{1 + C_{Ax}^2 + C_{Ay}^2}}$$

$$C_{Ax} = \frac{X_A - X_c}{N_H} \sin(FOV_x) \qquad C_{Ay} = \frac{Y_A - Y_c}{N_V} \sin(FOV_y)$$

where n_A is the aim-point unit vector and C the directional cosines, both referenced to the current missile heading

(X_C, Y_C). By transforming the aim-point vector and current missile heading into a fixed reference frame at each time frame, the track angle error is defined by the angular rotation of the aim-point vector into the current missile heading (n_v):

$$\Delta\vec{\theta}_{los} = \Delta\theta\ \vec{n}_\theta \qquad \Delta\theta = \cos^{-1}\left[\ \vec{n}_A \cdot \vec{n}_V\ \right] \qquad \vec{n}_\theta = \frac{\vec{n}_V \times \vec{n}_A}{\left|\ \vec{n}_V \times \vec{n}_A\ \right|}$$

The angular velocity of the track angle error (ω_{los}) and the proportional navigation law are used to compute the desired missile acceleration (a_M):

$$\vec{\omega}_{los} = \frac{\Delta\vec{\theta}_{los}(t) - \Delta\vec{\theta}_{los}(t-1)}{\Delta t} \qquad \vec{a}_M = \left\{ K_M \right\}^T \vec{\omega}_{los}$$

The angular velocity is first computed with respect to the fixed reference frame and then transformed with reference to the current missile heading in order to apply the yaw, pitch, and roll accelerations. Currently, the gain control constant is only applied to the yaw component, simulating a sea-skimming missile.

7. SCENARIO ANALYSIS

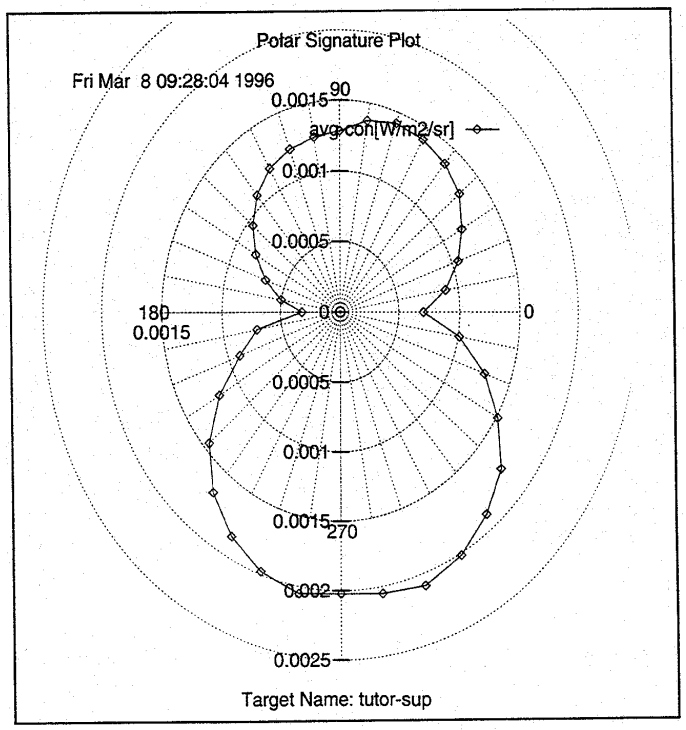

Figure 4: Average contrast radiance at 5 km.

When an NTCS scenario is loaded and configured, the resultant IR scene is displayed. The scene can be viewed in either wireframe, temperature or radiance, as illustrated in Figures 1 and 2. It is possible to change the observer position, line-of-sight and perspective interactively by using keyboard and mouse controls, or by entering values in a pop-up dialog. The analysis tools described in this section are used to evaluate the scenario for target signature,

detectability and survivability, as well as carry out engagement simulations.

7.1 Image analysis

An on-screen image analysis utility makes it possible to define any multi-sided (convex) polygon in the main image or use the entire window to compute various image statistics. In temperature mode, the mean temperature and surface area (normal to the observer at the target range) are computed. In radiance mode, the peak/average radiance, the peak/average contrast radiance and the solid angle subtended by the polygon are calculated. These results are useful for validating the thermal/IR models against measured data. Any scene component (target, plume or background) can be analyzed.

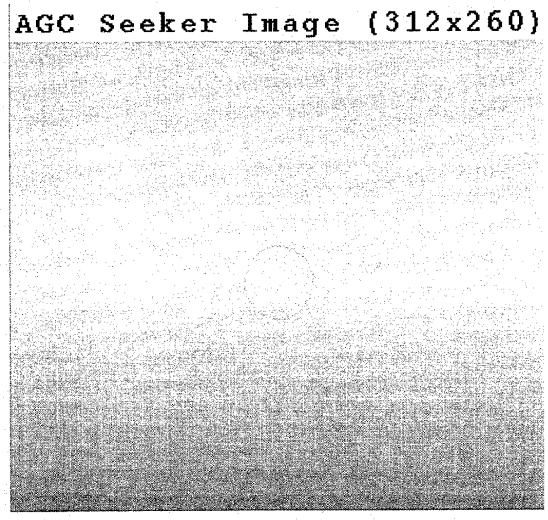

Figure 5: Target lock-on at horizon limit (18.5 km).

7.2 Polar signature

Using the same on-screen image tools, a number of azimuth steps are taken about a target at a specified range, altitude and field-of-view. The above radiance image statistics are computed at every step. The resultant data are viewed or printed as a polar signature plot. The average contrast radiance is the most useful of these and is illustrated in Figure 4. When multiplied by the solid angle ($E=L_{avg}x\omega$), these values represent the contrast irradiance emitted by a point-source target. The radiance values include the effects of atmospheric attenuation and observer-path radiance. Inspection of the polar signature plot reveals the variation in IR signature around the ship and the impact of solar heating. The sun in this image is at an elevation of 53° and azimuth of 336°, causing a 25% increase in contrast between the starboard and port sides of the ship. The lobe shape of the plot is caused by the largr surface area on the sides (90°,270°) compared with the bow and stern (0°,180°). The skewness in the plot towards the 0° axis is caused by increasing visibility of the forward-facing panels.

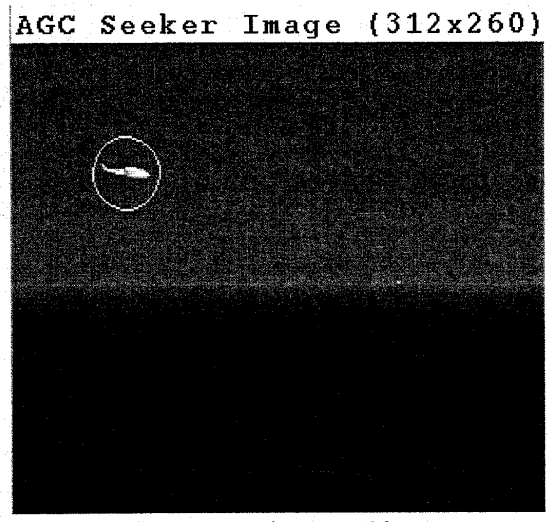

Figure 6: Helicopter enters image at 10 km.

7.3 Engagement simulation

The engagement simulation is a tactical development tool used to test the effectiveness of both infrared signature suppression and infrared flare countermeasures. The following is a hypothetical engagement scenario tested on NTCS. Figures 5 through 9 illustrate some of the screen captures taken from the seeker AGC image at key instances during the simulation. The missile is initially positioned at a range of 20 km from an unsuppressed ship, representing the initiation of terminal IR-guidance. Its heading is due South, with an altitude of 10 m, at a speed of 300 m/s. The ship is heading due East at a speed of 10 m/s. The seeker achieves a lock on the ship at the horizon (18.5 km), as shown in Figure 5. At 10 km, an unsuppressed helicopter, flying due West at 30 m/s, enters the seekers FOV and immediately becomes the seeker's aim-point, steering it away from the ship. Only 1 km in front of the missile, the contrast intensity of the helicopter is much larger than that of the ship. Although the missile is initially steered away from the ship, when the helicopter leaves the FOV at 9.4 km (Figure 7), the aim-point has moved closer to the ship and a lock on the ship is re-established (Figure 8). At 4.5 km, flare countermeasures are deployed behind the ship and the missile is steered away from the unsuppressed uptake and funnel. The current missile is not equipped with any counter-countermeasures.

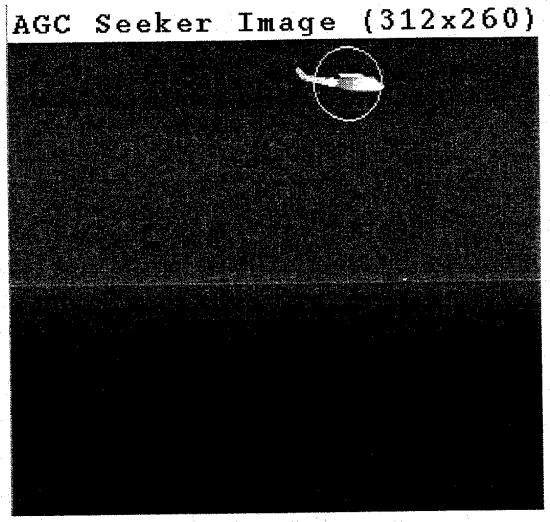

Figure 7: Helicopter leaving image at 9.4 km.

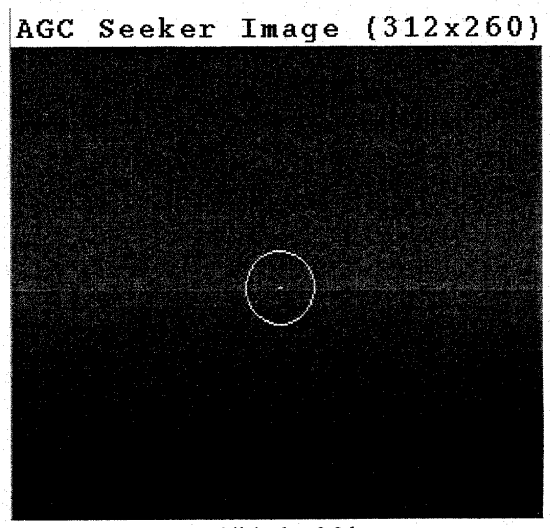

Figure 8: Lock re-established at 9.2 km

7.4 Polar lock-on range

A slightly modified version of the engagement simulation is used to predict polar lock-on ranges about a target. By specifying a number of azimuth steps and an initial range, the missile is flown along a constant heading towards the ship until its detection criteria are satisfied and a lock is established. Like polar signature analysis, it is carried out at every azimuth step and the results are viewed or printed as a polar plot (Figure 10). By changing the target signature, either through the application of IRSS or by changing the background conditions, reductions in susceptibility can be estimated from the changes in lock-on range.

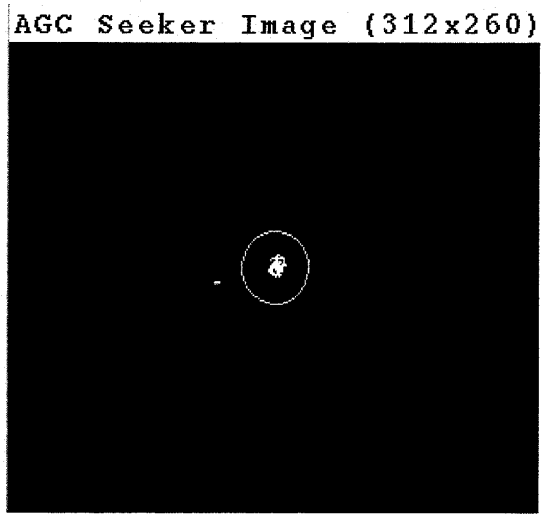

Figure 9: Flares launched at 4.5 km to deter missile.

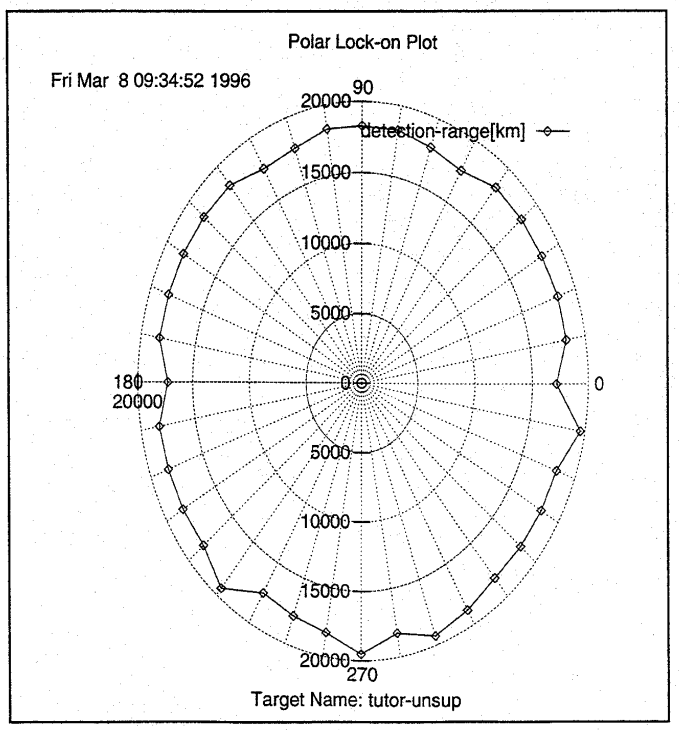

Figure 10: polar lock-on range for unsuppressed ship.

8. ACKNOWLEDGEMENTS

This work was performed under contract to the Canadian Department of National Defence under the technical authority of the Defence Research Establishment Valcartier (DREV). The authors wish to thank Mr. T.G. Brown of Spar Aerospace Ltd (Canada) for his contribution to the seeker head model.

9. REFERENCES

1. D.A. Vaitekunas, "SHIPIR: A naval ship infrared simulator - Volume I", *Technical Report, W.R. Davis Engineering Limited (file #A971), Department of Nation Defence - Defence Research Establishment (file #3713E-P111B)*, December 1992.
2. D.A. Vaitekunas, A.M. Birk and J. Morin, "SHIPIR: a naval ship infrared simulator", *Proceedings of the 1st Joint NATO-IRIS Symposium*, Gaithersburg, Maryland, July 14-16, 1992.
3. J. Morin, F. Reid and D.A. Vaitekunas, "SHIPIR: a model for simulating infrared images of ships at sea", *Proceedings of the SPIE Symposium*, Orlando, Florida, April 4-8, 1994.
4. D.A. Vaitekunas, K. Alexan, A.M. Birk and J. Morin, "Naval threat and countermeasure simulator", *Proceedings of the SPIE Symposium - Infrared Technology XX*, Vol. 2269, pp. 171-185, San Diego, California, July 25-28, 1994.
5. D.A. Vaitekunas and K. Alexan, "SHIPIR/NTCS - an integrated naval target, threat and countermeasure simulator", *Technical Report, W.R. Davis Engineering Limited (file #A501)*, December 1995.
6. F.X. Kneizys et al., "Atmospheric transmittance/radiance computer code LOWTRAN7", *Air Force Geophysics Laboratory, Report #AFGL-TR-88-0177*, Hanscom AFB, Massachusetts, August 1988.
7. A. Berk, L.S. Bernstein and D.C. Robertson, "MODTRAN: A moderate resolution model for LOWTRAN 7", *Geophysics Laboratory, Air Force Systems Command, United States Air Force, Report #GL-TR-89-0122*, Hanscom AFB, Massachusetts, April 1989.
8. C. Cox and W. Munk, "Measurement of the roughness of the sea surface from photographs of the sun's glitter", *J. Opt. Society Am.* Vol. 44, No. 11, p. 838-850, Nov. 1954.
9. P.M. Saunders, "Radiance of Sea and Sky in the Infrared Window 800-1200 cm^{-1}", *J. Opt. Society Am.*, Vol. 58, No. 5, p. 645-652, May 1968.
10. J.K. Lovin, A.W. Lubkowitz, and L.W. Spradley, "User's manual for RAVFAC, a radiation view factor digital computer program", *Lockheed Missiles and Space Company, Inc., Huntsville Research and Engineering Center*, Huntsville Research Park, Huntsville, Alabama, 1973.
11. R.D. Blevins, *Applied Fluid Dynamics Handbook*, Chapter 9, Van Nostrand Reinhold Company Inc, New York, 1984.
12. G.J. Baham and D. McCallum, "Stack design technology for naval and merchant ships", *SNAME Annual Meeting*, Paper No. 9, New York, N.Y., Nov. 10-12, 1977.
13. W. Romaniuk and A.M. Birk, "Development of an exhaust plume IR emission computer model", *W.R. Davis Engineering Ltd., Report C85-82*, 1988.
14. J. Morin, F. Reid and A. Morin, "An infrared ship/decoy/missile encounter model", *Proceedings of the SPIE Symposium*, Orlando, Florida, April 4-8, 1994.
15. Accetta, J.S., Shumaker, D.L., *The Infrared and Electro-Optical Systems Handbook*, SPIE Optical Engineering Press, 1993.